Origins of Negative and Positive Electromechanical Response of Oligopeptide Piezoelectrics

*Ni Nyoman D. Gayatri, Geoffrey R. Hutchison**

Department of Chemistry, University of Pittsburgh, 219 Parkman Avenue, Pittsburgh, PA 15260,

ABSTRACT In response to an applied electric field, materials and even individual molecules can exhibit electromechanical response. Previous work has demonstrated the piezoelectric distortion of polar organic crystals, biomaterials, and even single molecular monolayers, increasing length in response to the change in potential energy of interaction between the polarization or dipole moment and the applied electric field. In this work, we demonstrate through density functional calculations that helical oligopeptides, depending on sequence can exhibit both positive and surprisingly also negative piezoresponse. While the overall molecular dipole moment may favor positive piezoresponse, individual hydrogen bonding interactions along the backbone have the opposite direction, enabling tailored sequences to yield either net expansion or contraction in response to an electric field. While negative piezoresponse has largely been considered in polyvinylidene difluoride (PVDF) and related systems, understanding the atomic and molecular basis for both electromechanical effects will yield interesting new applications.

TOC GRAPHIC

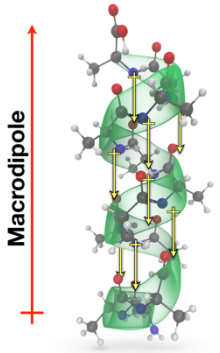

Introduction

Piezoelectric materials generate electric charge in response to physical stresses (the direct piezoelectric effect) or through deformation under an electric field (the inverse piezoelectric effect). Due to this property of piezoelectric materials, they have caught the attention of researchers who are interested in improving energy efficiency through a different method of energy harvesting. For example, piezoelectric materials find wide uses ranging from consumers to medical applications such as force sensors[1], actuators[1], and pacemakers[2]. On the other hand, a piezoelectric actuator directly converts an electrical signal into a precisely controlled physical displacement. For example, medical implant devices use piezoelectric responses to monitor temperature or blood pressure.[3] Piezoelectric motors can be powered by converting the vibrations of piezoelectric materials[4] for applications such navigating through the bloodstream.

The geometric change of a material in the presence of electric fields determines the piezoresponse of a material. To date, the most highly responsive piezo materials are ceramics (e.g., lead zirconium titanate, PZT) and semi-crystalline polymers such as polyvinylidene difluoride (PVDF).[5] While a piezoresponse is found in many polar inorganic materials, the piezoelectric effect is also found in a number of biomaterials such as peptides and amino acids. The assembly of proteins show adaptation due to environment changes (for example redox, pH, and chemical gradient), and these characteristics extend to applied electric fields.[5] For example, collagen,[6] viruses,[7] aligned peptide crystals,[8] horse muscle,[9] fish scales,[10] and peptide nanotubes,[11] exhibit

piezoresponse in prior studies. Despite both experimental and computational studies, full understanding of what molecular properties yield large piezo response does not yet exist.

Previous computational studies have demonstrated the piezoelectric effect in hydrogen-bonded molecules[7, 12-13] and individual molecules.[7] Recent experimental studies have measured piezo response in individual molecular monolayers using piezo force microscopy.[5] While such experiments have demonstrated the effect of molecular flexibility on piezoresponse in oligopeptides, computational studies can guide further experimental investigation, including the effect of amino acid side chains on piezo response.

In this work, we particularly focus on substitutions with two particular amino acids: tyrosine and phenylalanine in helical oligoalanine backbones. Both add polarizable aromatic phenyl rings, potentially increasing the electrostatic molecular response to an applied electric field. The sole difference is in the additional hydrogen bonding -OH group in tyrosine. Additionally, the effects of oligopeptide length and repeated phenylalanine or tyrosine substitutions will be considered.

Computational Methods

Adopting methods from our previous work on π-conjugated helicenes,[7] all molecular geometries were optimized using the B3LYP density functional[14-15] and the 6-31G(d) basis set using Gaussian 09.[16] While little experimental data is yet available for comparison with computed piezoelectric response, the B3LYP functional has generally been the method of choice for accurate molecular geometries, and focus mainly on the structure/property trends with the computed geometric deformations.[17-18] When our group compared computed to experimental piezoelectric coefficients of crystalline 2-methyl-4-nitroaniline, high agreement was found between computational and experimental piezoelectric responses (in hydrogen bonding interactions) when using the B3LYP functional.[19] Since DFT methods are known to be asymptotically incorrect and ignore dispersion,[20-26] we also tested results with the ω-B97X-D3 functional.[27]

All oligopeptides are indicating using standard three-letter abbreviations, for example Tyr_3-Ala_5 (Scheme 1), represents the neutral peptide aligned along the x-axis, with the origin at the terminal NH_2 group, and the tyrosine residues at the bottom of the peptide structure. Each sequence investigated is compiled in Table S1. For the present study, initial geometries were generated using the Avogadro molecular editor,[18] assuming a helical secondary structure, followed by density functional optimization as described above.

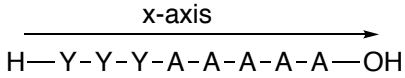

Scheme 1. Amino acid notation of Tyr3-Ala5 sequence which was optimized on x-direction.

As in our previous work, the molecular geometry is oriented to a specific frame of reference (i.e., aligned along the Cartesian x-axis) using Avogadro[18] or a custom Python script (see Supporting Information), and the geometry was optimized under different applied electric fields along the molecular (x) axis. The molecular length after optimization under each electric field was used to calculate piezocoefficient (d_{33}).

The piezoelectric coefficient is a tensor derived from the direction of the applied field and the resulting molecular geometric distortion.[28] We restrict our discussion to the largest such contribution, and the piezoelectric coefficient, d_{33}, was calculated from the molecular length at maximum extension (l_{max}) and at zero applied field (l_{zero}) using Equation 1:

$$d_{33}\left[\frac{pm}{V}\right] = \frac{(l_{max}-l_{min})}{(l_{zero})} \times \frac{1}{field}\left[\frac{nm}{V}\right] \times 1000\left[\frac{pm}{nm}\right] \quad (1)$$

Note that while this formula suggests a linear response of the piezoelectric distortion to the applied electric field, there is no guarantee that all molecules will exhibit linear electromechanical responses.

For example, Figure 1 displays the deformation of the Phe_3-Ala_5 oligopeptide sequence under different applied electric fields. As we increase the field strength, the Phe_3-Ala_5 oligopeptide increases in length, yielding a computed piezo response of 15.23 pm/V. Meanwhile, Figure 2 displays the deformation of the Ala_9-Phe_3 oligopeptide sequence under applied electric fields. As

we increase the field strength, this oligopeptide contracts, yielding a computed piezo response of -0.75 pm/V.

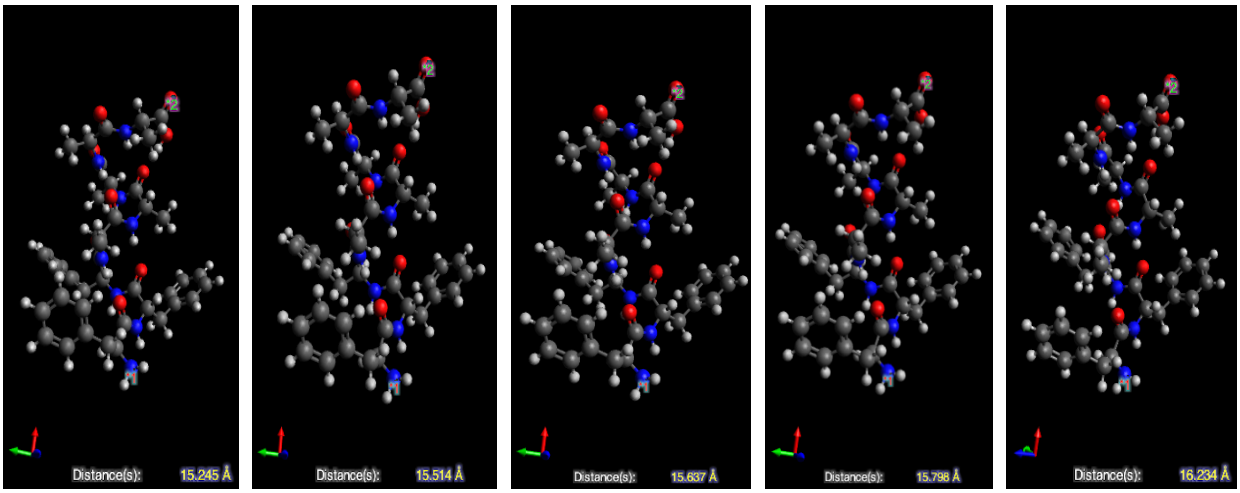

-0.51 V/nm	-0.26 V/nm	0 V/m	+0.26 V/nm	+0.51 V/nm
15.25 Å	15.51 Å	15.64 Å	15.80 Å	16.23 Å

Figure 1. B3LYP-optimized geometries of Phe_3-Ala_5 with varied applied electric fields, with the N to O distance indicated. Note that the molecule extends with increasing electric field, reflecting a positive d_{33} piezo response (15.23 pm/V).

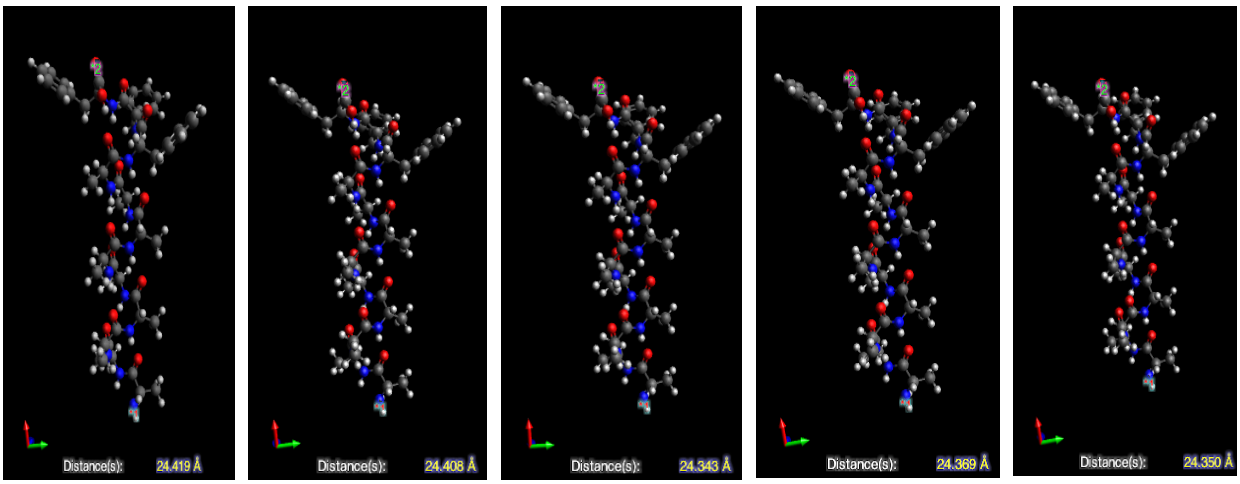

-0.51 V/nm	-0.26 V/nm	0 V/m	+0.26 V/nm	+0.51 V/nm
24.42 Å	24.41 Å	24.34 Å	24.37 Å	24.35 Å

Figure 2. B3LYP-optimized geometries of Ala_9-Phe_3 with varied applied electric fields, with the N to O distance indicated. Note that with the same alignment, the molecule contracts with increasing electric field, reflecting a negative piezo response (-0.75 pm/V).

Multiple helical oligopeptide sequences were studied, including both tyrosine (Tyr) and phenylalaine (Phe) substitution of oligoalanines to consider the effect of polarizable side chains. The number of amino acids along the helix is also varied from 8 to 14 residues. All sequences and naming conventions are compiled in Table S1.

Results and Discussion

The overall purpose of this study is to understand the molecular properties of peptides that give rise to a large piezoresponse by simulating the deformation of helical oligopeptide structures. In particular, the use of tyrosine and phenylalanine side chains should introduce polarizable side chains, presumably increasing the induced dipole moment under applied field and thus the electrostatic interaction involved in piezo response of the peptides. Such Tyr and Phe substitutions will be considered at the top (C-terminus), at the bottom (N-terminus) as well as in the middle of the sequence of alanine residues.

Based on the optimized geometries under an applied electric field (e.g., Figures 1 and 2), one can compute a piezo response using Equation 1 (i.e., from the slope of the distance-field plots in Figure 3). Surprisingly, different sequences yield completely different *signs* of the piezo response: from a large positive response (expansion) to a small negative response (contraction).

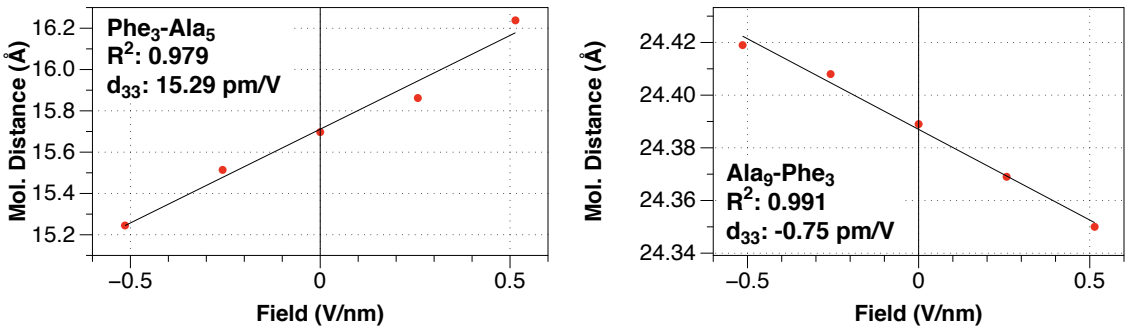

Figure 3. Plots of the length of the optimized geometries from peptide sequence (left) Phe_3-Ala_5 with positive piezocoefficient and (right) Ala_9-Phe_3 with negative piezo coefficient calculated using B3LYP.

To understand the effect of substitution on piezo response, first three Phe or Tyr resiudes were substituted at the bottom (N-terminus) of the sequences. As illustrated in Figure 4, the B3LYP-computed d_{33} are compared as a function of sequence length and side-chain substitution. In general, both Phe and Tyr-substituted sequences show similar computed piezo response. The largest piezo response of +15.29 pm/V is found in Phe_3-Ala_5 structures (at eight residues), followed by Tyr_3-Ala_5 (at eight residues) with +14.68 pm/V. In one case, Phe_3-Ala_9 yields negative piezo response of -0.61 pm/V.

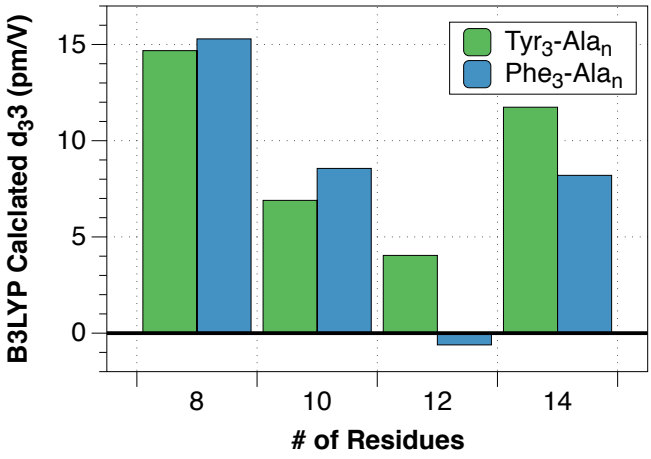

Figure 4. The resulting B3LYP-computed d_{33} obtained from phenylalanine and tyrosine substitutions at the bottom of the peptide structure (N terminus) e.g., Phe_3-Ala_n or Tyr_3-Ala_n.

Similarly, the B3LYP-computed piezo response was considered for substitution at the top (C-terminus) of the sequences (Figure 5). The largest positive piezo-coefficient of +7.7 pm/V is found in Ala_{11}-Phe_3 with a similarly large positive response in Ala_5-Tyr_3 (+7.46 pm/V). On the other hand, both types of substitutions show very small positive and negative piezo response at 8 residues, 10 residues, and 12 residues. Interestingly, both Phe and Tyr substitutions exhibit negative piezo-coefficient of -0.75 pm/V is found with Ala_9-Phe_3 (at 12 residues) and -0.73 pm/V is found with Ala_9-Tyr_3. Given only two outliers yielding strong positive piezo response, the C-terminal substitutions evidently strongly decrease the computed response. Even in the case of

Ala_{11}-Phe_3 and Ala_5-Tyr_3, the computed response is much smaller than the corresponding N-terminal substitutions (Figure 4).

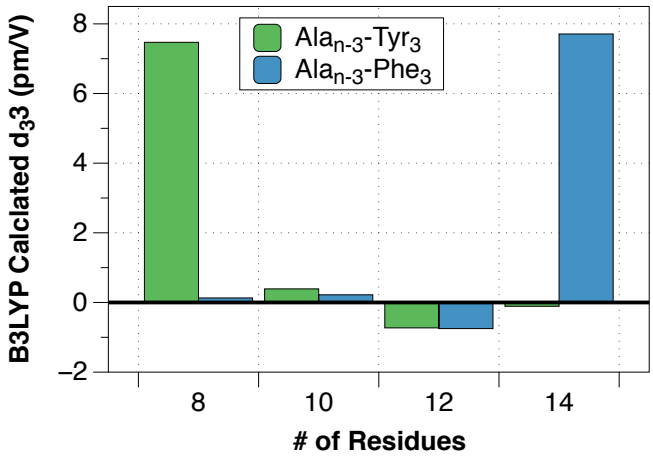

Figure 5. The resulting d_{33} obtained from phenylalanine and tyrosine with added residues. Both phenylalanine and tyrosine are located at the top of the peptide structure, (C terminus) e.g., Ala_n-Phe_3 or Ala_n-Tyr_3.

Given the small electromechanical deformations with C-terminal substitutions, clearly the overall molecular length does not show significant distortion. Smaller local effects may occur, for example between the C=O and NH hydrogen-bonding interactions along the helix, since those have been previously found to exhibit piezo response.[29-31] In Figure 6, the average distance between O and N hydrogen-bonding neighbors for Phe_3-Ala_5 and Ala_9-Phe_3 are compared as a function of electric field strength. The plot shows a *negative* linear trend (i.e., contraction) for both sequences. Despite the different overall piezo response from the two molecules, the hydrogen bonds contract, consistent with recent analysis of negative piezo response in hydrogen bond pairs.[29]

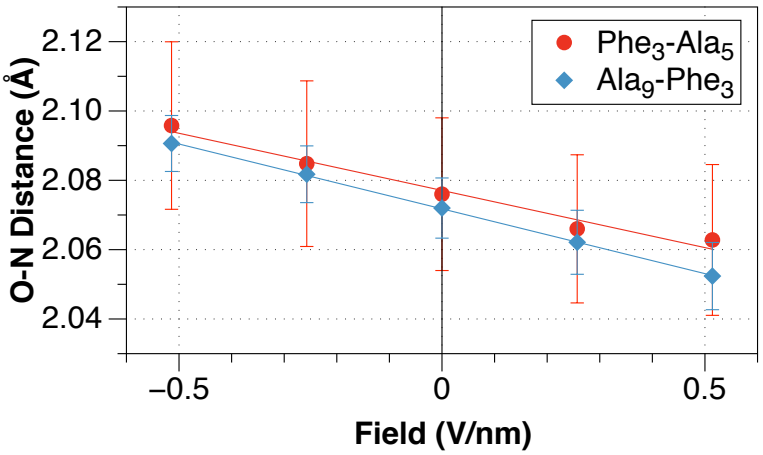

Figure 6. Average O-N hydrogen bond distances obtained from along the oligopeptides Phe_3-Ala_5 and Ala_9-Phe_3.

Since the hydrogen bonds contract with similar trends regardless of the sequence, one might wonder how the overall piezo response still favor positive expansion. The macrodipole along the helix strongly interacts with the applied electric field, producing potential energy driving towards an expanded length. These effects can be revealed through the backbone torsion angles ϕ and φ. Using a Python script to extract the Ramachandran angles, Figure 7 illustrates that the ϕ backbone angles from B3LYP-computed optimized geometries change significantly as a function of applied field strength in both oligopeptides with positive and negative computed piezo response. In the case of a ϕ backbone angle shift from ~61° to ~59°, the helix elongates with increasing applied electric field (i.e., a positive piezo response from the helix macrodipole coupling to the field).

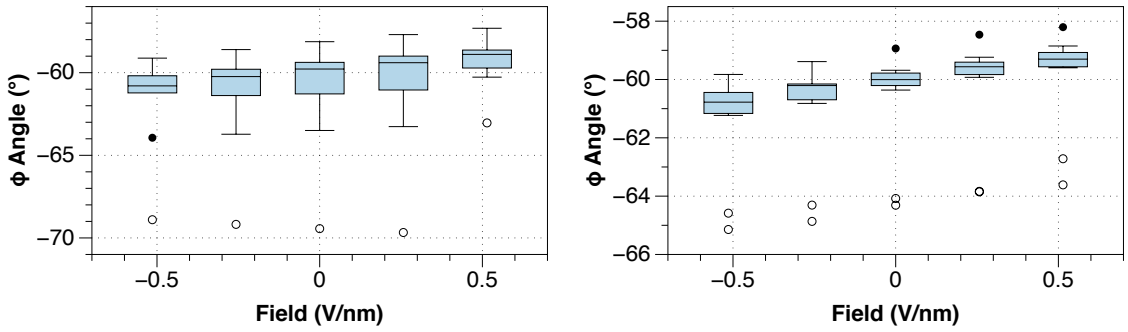

Figure 7. Ramachandran angle ϕ for B3LYP-optimized geometries of (left) Tyr_3-Ala_{11} and (right) Ala_{11}-Tyr_3 as a function of applied electric field.

The geometric comparisons in Figures 6 and 7 illustrate that regardless of the overall computed piezo response (i.e., positive or negative), the peptide sequences respond in similar ways to the applied electric fields. The hydrogen bonds contract slightly with positive electric fields, consistent with negative piezo response.[29] At the same time, the ϕ dihedral angles along the chain twist towards less negative values (i.e. a longer helix). In the case of top-substituted C-terminal sequences, steric hindrance evidently results in a trend towards negative overall piezo response (e.g., Ala_9-Phe_3 in Figures 2 and 3).

Consequently, sequences with "middle" substitutions were also considered, for example, Ala-Tyr-Ala and Ala-Phe-Ala, in which the two types of side chains are buried inside the oligoalanine helix (Figure 8), nearer to the bottom of the sequence (N-terminus) or nearer to the C-terminus. Note that, both phenylalanine and tyrosine have similar trends. The largest piezo-coefficient is found in Ala-Phe_3-Ala_4 (at eight residues), $d_{33} \approx 15.40$ pm/V, with response typically decreasing with sequence length. In all cases, the computed piezo response is positive, although substitutition near the C-terminus with eight- and ten-residue sequences yields smaller computed response than the corresponding N-terminus.

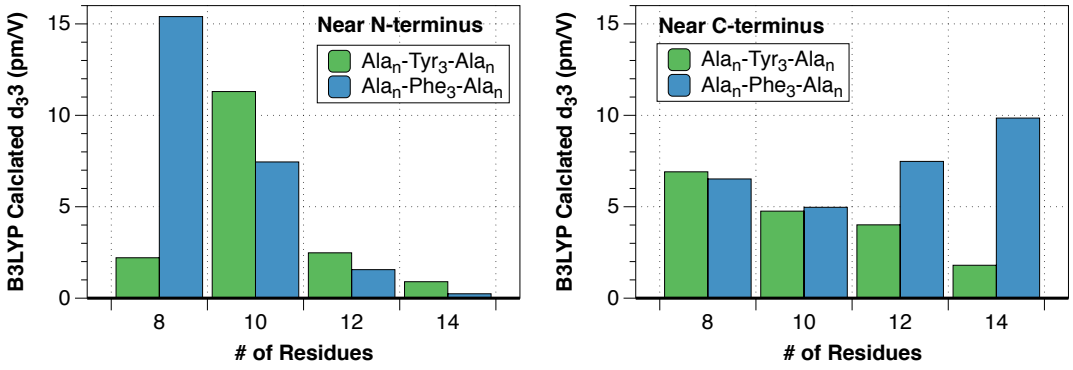

Figure 8. Computed B3LYP d_{33} piezo response as a function of oligopeptide length and "internal" side chain substitution closer to the (left) N-terminus e.g., Ala-Tyr_3-Ala_4, Ala-Phe_3-Ala_4, Ala_2-Tyr_3-Ala_5, Ala_2-Phe_3-Ala_4, etc., or (right) C-terminus, e.g., Ala_4-Tyr_3-Ala, Ala_4-Phe_3-Ala, Ala_5-Tyr_3-Ala_2, Ala_5-Phe_3-Ala_2 etc.

Conclusions

Using density functional optimized geometries of oligopeptides in response to applied electric fields along the peptide helix, the deformation of sequences containing alanine, phenylalanine, and tyrosine were compared. The length of the oligopeptides and the nature of the sequences yielded both positive and negative piezoresponse. Some variability between particular sequences likely occurs from the large number of geometry optimization calculations with large molecules – with many local minima. Although every effort was made to ensure all geometries are the global minima for the sequence and applied field, some errors may occur.

Overall, we note very similar computed piezo coefficients from both Tyr and Phe substitutions and no clear effect of sequence length on piezo response. On the other hand, we find that two measures of structural distortion – the distance between O and NH hydrogen bond atoms along the helix, and the ϕ backbone angles show opposing trends. That is, the local effects of hydrogen bonds act to *contract* the oligopeptide sequence (i.e., a *negative* piezo response) matching recent research on the electromechanical response of h-bonds.[29] At the same time, the macrodipole associated with the helical secondary structure push the backbone angles to elongate, a *positive* piezo response. In cases with Tyr or Phe substitution near the C-terminus, this latter effect is diminished, reflecting an overall negative piezo contraction (e.g., Figures 2, 3, 5). In remaining cases with substitution near the N-terminus or internal substitution, the overall piezo response is positive, with d_{33} piezo coefficients only slightly smaller than PVDF.

There is an increasing interest in the electromechanical response of organic and biomaterials,[5, 32-33] and computational design of peptides with increased response will guide efforts to produce new active materials for applications including touch and force sensors, and electroactive actuators.

ACKNOWLEDGMENT This research was conducted in part through the AP Capstone program at Pittsburgh Allderdice high school. N. G. gratefully acknowledges all those who were involved in supporting this research project, including Dr. Janet Waldeck. Funding for G.R.H. was provided by the National Science Foundation (DMR-1608725). This research was supported in part by the University of Pittsburgh Center for Research Computing through the computational resources provided.

REFERENCES

1. Bosne, E. D.; Heredia, A.; Kopyl, S.; Karpinsky, D. V.; Pinto, A. G.; Kholkin, A. L., Piezoelectric Resonators Based on Self-Assembled Diphenylalanine Microtubes. *Appl Phys Lett* **2013**, *102*.
2. Chorsi, M. T.; Curry, E. J.; Chorsi, H. T.; Das, R.; Baroody, J.; Purohit, P. K.; Ilies, H.; Nguyen, T. D., Piezoelectric Biomaterials for Sensors and Actuators. *Adv Mater* **2019**, *31*.
3. Dagdeviren, C., et al., Conformal Piezoelectric Energy Harvesting and Storage from Motions of the Heart, Lung, and Diaphragm. *Proc Natl Acad Sci U S A* **2014**, *111*, 1927-32.
4. Watson, B. F., James P.; Yeo, Leslie Y., Piezoelectric Ultrasonic Resonant Motor with Stator Diameter Less Than 250 Mm: The Proteus Motor. *Journal of Micromechanics and Microengineering* **2009**, *19*.
5. Marvin, C. W.; Grimm, H. M.; Miller, N. C.; Horne, W. S.; Hutchison, G. R., Interplay among Sequence, Folding Propensity, and Bio-Piezoelectric Response in Short Peptides and Peptoids. *Journal of Physical Chemistry B* **2017**, *121*, 10269-10275.
6. Ahn, A. C.; Grodzinsky, A. J., Relevance of Collagen Piezoelectricity to "Wolff's Law": A Critical Review. *Med Eng Phys* **2009**, *31*, 733-741.
7. Quan, X. F.; Marvin, C. W.; Seebald, L.; Hutchison, G. R., Single-Molecule Piezoelectric Deformation: Rational Design from First-Principles Calculations. *J Phys Chem C* **2013**, *117*, 16783-16790.
8. Horiuchi, S.; Tsutsumi, J.; Kobayashi, K.; Kumai, R.; Ishibashi, S., Piezoelectricity of Strongly Polarized Ferroelectrics in Prototropic Organic Crystals. *J Mater Chem C* **2018**, *6*, 4714-4719.
9. Nguyen, V.; Zhu, R.; Jenkins, K.; Yang, R. S., Self-Assembly of Diphenylalanine Peptide with Controlled Polarization for Power Generation. *Nat Commun* **2016**, *7*.
10. Ghosh, S. K.; Mandal, D., High-Performance Bio-Piezoelectric Nanogenerator Made with Fish Scale. *Appl Phys Lett* **2016**, *109*, 232-236.
11. Kholkin, A.; Amdursky, N.; Bdikin, I.; Gazit, E.; Rosenman, G., Strong Piezoelectricity in Bioinspired Peptide Nanotubes. *Acs Nano* **2010**, *4*, 610-614.
12. Werling, K. A.; Griffin, M.; Hutchison, G. R.; Lambrecht, D. S., Piezoelectric Hydrogen Bonding: Computational Screening for a Design Rationale. *J Phys Chem A* **2014**, *118*, 7404-7410.

13. Calio, R.; Rongala, U. B.; Camboni, D.; Milazzo, M.; Stefanini, C.; de Petris, G.; Oddo, C. M., Piezoelectric Energy Harvesting Solutions. *Sensors-Basel* **2014**, *14*, 4755-4790.
14. Becke, A. D., Density-Functional Thermochemistry .5. Systematic Optimization of Exchange-Correlation Functionals. *J Chem Phys* **1997**, *107*, 8554-8560.
15. Lee, C. T.; Yang, W. T.; Parr, R. G., Development of the Colle-Salvetti Correlation-Energy Formula into a Functional of the Electron-Density. *Phys Rev B* **1988**, *37*, 785-789.
16. Frisch, M. J.; Trucks, G.; Schlegel, H.; Scuseria, G.; Robb, M.; Cheeseman, J.; Scalmani, G.; Barone, V.; Mennucci, B.; Petersson, G., Gaussian 09, Revision D. 01, Gaussian. *Inc.: Wallingford, CT* **2009**.
17. Hickey, A. L.; Rowley, C. N., Benchmarking Quantum Chemical Methods for the Calculation of Molecular Dipole Moments and Polarizabilities. *J Phys Chem A* **2014**, *118*, 3678-3687.
18. Hanwell, M. D.; Curtis, D. E.; Lonie, D. C.; Vandermeersch, T.; Zurek, E.; Hutchison, G. R., Avogadro: An Advanced Semantic Chemical Editor, Visualization, and Analysis Platform. *J Cheminformatics* **2012**, *4*.
19. Werling, K. A.; Hutchison, G. R.; Lambrecht, D. S., Piezoelectric Effects of Applied Electric Fields on Hydrogen-Bond Interactions: First-Principles Electronic Structure Investigation of Weak Electrostatic Interactions. *J Phys Chem Lett* **2013**, *4*, 1365-1370.
20. Grimme, S.; Antony, J.; Ehrlich, S.; Krieg, H., A Consistent and Accurate Ab Initio Parametrization of Density Functional Dispersion Correction (Dft-D) for the 94 Elements H-Pu. *J Chem Phys* **2010**, *132*.
21. Swart, M.; Sola, M.; Bickelhaupt, F. M., Inter- and Intramolecular Dispersion Interactions. *J Comput Chem* **2011**, *32*, 1117-1127.
22. Ehrlich, S.; Bettinger, H. F.; Grimme, S., Dispersion-Driven Conformational Isomerism in Sigma-Bonded Dimers of Larger Acenes. *Angew Chem Int Edit* **2013**, *52*, 10892-10895.
23. Cai, Z. L.; Sendt, K.; Reimers, J. R., Failure of Density-Functional Theory and Time-Dependent Density-Functional Theory for Large Extended Pi Systems. *J Chem Phys* **2002**, *117*, 5543-5549.
24. Kohn, W.; Meir, Y.; Makarov, D. E., Vanderwaals Energies in Density Functional Theory. *Phys Rev Lett* **1998**, *80*, 4153-4156.
25. Baer, R.; Neuhauser, D., Density Functional Theory with Correct Long-Range Asymptotic Behavior. *Phys Rev Lett* **2005**, *94*.
26. Gritsenko, O.; Baerends, E. J., Asymptotic Correction of the Exchange-Correlation Kernel of Time-Dependent Density Functional Theory for Long-Range Charge-Transfer Excitations. *J Chem Phys* **2004**, *121*, 655-660.
27. Chai, J. D.; Head-Gordon, M., Long-Range Corrected Hybrid Density Functionals with Damped Atom-Atom Dispersion Corrections. *Phys Chem Chem Phys* **2008**, *10*, 6615-6620.
28. Werling, K. A.; Hutchison, G. R.; Lambrecht, D. S., Developing a Molecular Theory of Electromechanical Responses. *arXiv* **2017**, 1707.07464.
29. Werling, K. A.; Lambrecht, D.; Hutchison, G. R., Molecular Origin of Positive and Negative Electromechanical Response in Hydrogen-Bonded Systems. *ChemRxiv* **2019**, doi: 10.26434/chemrxiv.9943640.v1.
30. Werling, K. A.; Hutchison, G.; Lambrecht, D. S., Piezoelectric Effects of Applied Electric Fields on Hydrogen-Bond Interactions: First-Principles Electronic Structure Investigation of Weak Electrostatic Interactions. *Journal of Physical Chemistry Letters* **2013**, *4*, 1365-1370.
31. Werling, K. A.; Griffin, M.; Hutchison, G. R.; Lambrecht, D. S., Piezoelectric Hydrogen Bonding: Computational Screening for a Design Rationale. *Journal of Physical Chemistry A* **2014**, *118*, 7404–7410.
32. Stetsovych, O., et al., Large Converse Piezoelectric Effect Measured on a Single Molecule on a Metallic Surface. *Journal of the American Chemical Society* **2018**, *140*, 940-946.

33. Quan, X.; Marvin, C. W.; Seebald, L.; Hutchison, G. R., Single-Molecule Piezoelectric Deformation: Rational Design from First-Principles Calculations. *Journal of Physical Chemistry C* **2013**, *117*, 16783-16790.

ASSOCIATED CONTENT

Table S1. Naming convention of peptide sequences which were considered in this work.

Peptide Sequence	**Amino Acid Notation**
Tyr3-Ala5	H_2N-Y-Y-Y-A-A-A-A-A-CO_2H
Tyr3-Ala7	H_2N-Y-Y-Y-A-A-A-A-A-A-A-CO_2H
Tyr3-Ala9	H_2N-Y-Y-Y-A-A-A-A-A-A-A-A-A-CO_2H
Tyr3-Ala11	H_2N-Y-Y-Y-A-A-A-A-A-A-A-A-A-A-A-CO_2H
Ala5-Tyr3	H_2N-A-A-A-A-A-Y-Y-Y-CO_2H
Ala7-Tyr3	H_2N-A-A-A-A-A-A-A-Y-Y-Y-CO_2H
Ala9-Tyr3	H_2N-A-A-A-A-A-A-A-A-A-Y-Y-Y-CO_2H
Ala11-Tyr3	H_2N-A-A-A-A-A-A-A-A-A-A-A-Y-Y-Y-CO_2H
Phe3-Ala-5	H_2N-F-F-F-A-A-A-A-A-CO_2H
Phe3-Ala7	H_2N-F-F-F-A-A-A-A-A-A-A-CO_2H
Phe3-Ala9	H_2N-F-F-F-A-A-A-A-A-A-A-A-A-CO_2H
Phe3-Ala11	H_2N-F-F-F-A-A-A-A-A-A-A-A-A-A-A-CO_2H
Ala5-Phe3	H_2N-A-A-A-A-A-F-F-F-CO_2H
Ala7-Phe3	H_2N-A-A-A-A-A-A-A-F-F-F-CO_2H
Ala9-Phe3	H_2N-A-A-A-A-A-A-A-A-A-F-F-F-CO_2H
Ala11-Phe3	H_2N-A-A-A-A-A-A-A-A-A-A-A-F-F-F-CO_2H
Ala1-Tyr3-Ala4	H_2N-A-Y-Y-Y-A-A-A-A-CO_2H
Ala2-Tyr3-Ala5	H_2N-A-A-Y-Y-Y-A-A-A-A-A-CO_2H
Ala3-Tyr3-Ala6	H_2N- A-A-A-Y-Y-Y-A-A-A-A-A-A-CO_2H
Ala4-Tyr3-Ala7	H_2N-A-A-A-A-Y-Y-Y-A-A-A-A-A-A-A-CO_2H
Ala4-Tyr3-Ala1	H_2N-A-A-A-A-Y-Y-Y-A-CO_2H
Ala5-Tyr3-Ala2	H_2N-A-A-A-A-A-Y-Y-Y-A-A-CO_2H
Ala6-Tyr3-Ala3	H_2N-A-A-A-A-A-A-Y-Y-Y-A-A-A-CO_2H
Ala7-Tyr3-Ala4	H_2N-A-A-A-A-A-A-A-Y-Y-Y-A-A-A-A-CO_2H
Ala1-Phe3-Ala4	H_2N-A-F-F-F-A-A-A-A-CO_2H
Ala2-Phe3-Ala5	H_2N-A-A-F-F-F-A-A-A-A-A-CO_2H
Ala3-Phe3-Ala6	H_2N- A-A-A-F-F-F-A-A-A-A-A-A-CO_2H
Ala4-Phe3-Ala7	H_2N-A-A-A-A-F-F-F-A-A-A-A-A-A-A-CO_2H
Ala4-Phe3-Ala1	H_2N-A-A-A-A-F-F-F-A-CO_2H
Ala5-Phe3-Ala2	H_2N-A-A-A-A-A-F-F-F-A-A-CO_2H
Ala6-Phe3-Ala3	H_2N-A-A-A-A-A-A-F-F-F-A-A-A-CO_2H
Ala7-Phe3-Ala4	H_2N-A-A-A-A-A-A-A-F-F-F-A-A-A-A-CO_2H